Textural and chemical features of a “soft” plug emitted during Strombolian explosions: A case study from Stromboli volcano

A. Caracciolo, Lucia Gurioli, P. Marianelli, Bernard Julien, A. Harris

Textural and chemical features of a "soft" plug emitted during strombolian explosions: a case study from Stromboli volcano

A. Caracciolo[1, 2, 3], L. Gurioli[2], P. Marianelli[3], J. Bernard[2, 4], A. Harris[2]

Corresponding author: alberto@hi.is

1. Institute and Faculty of Earth Sciences, University of Iceland, Sturlugata 7, 101 Reykjavık, Iceland

2. Laboratoire Magmas et Volcans, Université Clermont Auvergne - CNRS - IRD, OPGC, Campus Universitaire des Cézeaux, 6 Avenue Blaise Pascal, TSA 60026 - CS 60026, 63178 AUBIERE Cedex, France

3. Dipartimento di Scienze della Terra, Università di Pisa, via Santa Maria 53, 56126 Pisa, Italy

4. Bureau de Recherche Géologique et Minière (BRGM), UMR 7327, 3 avenue Claude Guillemin, BP 36009, 45060 Orléans Cedex 2, France

Abstract

Between May 2009 and March 2010, six small scale paroxysms were recorded at Stromboli volcano (Aeolian Islands, Italy). The small scale paroxysm of 21 January 2010 was the only one characterized by a SSE to SW dispersal direction, which allowed access for sampling of the associated bomb-dominated deposit. The quenched marginal portions of twelve bombs were used to perform density, textural and chemical analyses to define the mechanisms operating in the shallow conduit during the explosion. Whole-rock density values span a range of 1100 to 2300 kg/m^3 which, using a dense rock equivalent density of 2850 kg/m^3, converts to a vesicularity of 20 to 61 %. The vesicle volume distribution (VVD) is unimodal, with a mode at 1.8 mm, consistent with a single bubble nucleation event followed by growth, coalescence expansion and/or densification. Crystallinity ranges from 30-62 vol. %. Vesicle and crystal contents, however, show considerable

variation, consistent with the presence of an extremely dense and degassed component in the fragmented magma. Both groundmass glasses and melt inclusions are chemically homogenous, with CaO/Al_2O_3 in the range 0.40-0.60. Melt inclusion volatile contents (H_2O up to 0.47 wt%) are consistent with fragmentation of a shallow magma residing at a depth of about 480 m. We suggest that dense, degassed and crystal-rich magma formed a "soft" rheological plug at the top of the conduit. Under such a condition, bubbles can accumulate under the plug to slowly build the pressure to a threshold point, after which the pressure is enough to cause the fragmentation of the plug.

Key words: Strombolian explosions, conduit-capping plug, degassed bombs, melt inclusions, small scale paroxysms

1. Introduction

Stromboli, a 924 m high volcanic island located in the Aeolian archipelago of the Southern Tyrrhenian Sea (Fig. 1), is famous for its persistent state of activity that has been on-going since the medieval period (Rosi et al., 2000). All explosive eruptions occur in the crater terrace at 750 m a.s.l, where the three main active craters are located (Fig. 1) (Harris and Ripepe, 2007a). Normal explosive eruptions at Stromboli have been long-used to define the Strombolian sub-type of explosive activity and typically involve 10^2-10^3 kg of material (Harris et al., 2013) in repeated emissions of gas, bombs, lapilli and ash in events that last a few to tens of seconds (Barberi et al., 1993; Rosi et al., 2013; Houghton et al., 2016). Because of the variety of the ejected material associated with explosive events, normal activity at Stromboli has been subdivided in four main groups: type 0 events are gas jets carrying a very few small particles at high velocity (Leduc et al., 2015; Gaudin et al., 2017); type 1 events are dominated by emission of ballistic coarse particles; type 2a eruptions involve ash-rich plumes with large numbers of ballistics, and type 2b events are characterized prevalently by ash (Patrick et al., 2007; Harris et al., 2013). Volcanic activity at the Crater Terrace also involves continuous degassing (Pering et al., 2016) and gas puffing (Ripepe et

al., 1996; Harris and Ripepe, 2007a; Gaudin et al., 2017), as well as emission of lava flows (e.g. Calvari et al., 2008; Rosi et al. 2013). The explosive plumes associated with normal activity ascend to no more than 500 m, causing a discontinuous deposit of lapilli, bombs and/or coarse ash within 50-400 m of the vent (Harris and Ripepe, 2007a; Patrick et al., 2007; Rosi et al. 2013; Gurioli et al., 2014). This activity has typically been associated with the bursting of large bubbles of gas at the surface of the magma column (Parfitt, 2004) to expel a mixture of gas loaded with particles (Bombrun et al., 2015). Thus, while Stromboli itself has become synonymous with this mildly explosive, yet globally common, eruption style, fragmentation conditions and shallow conduit dynamics at Stromboli have also become intimately linked to those driving "Strombolian" activity.

Recently, the simple Strombolian eruption model whereby large slugs of gas ascend through liquid resident in the conduit to burst at the surface (Jaupart and Vergniolle, 1989) has been challenged due to the presence of ejecta with moderate-to-high crystallinity. While pyroclasts at Stromboli have 40 to 55 vol% of crystals (Métrich et al., 2010; Gurioli et al. 2014), those at Etna have >55 vol% (Polacci et al., 2006), and crystallinities of 30-40 vol% have been found at Yasur volcano, Vanuatu (Métrich et al., 2011). These crystal contents create rheological conditions that are close to the "eruptibility" limit for magmas (Marsh 1981). The presence of a highly viscous (10^5-10^6 Pa s), crystal-rich magma has thus motivated the generation of new models to explain the passage of the slug through a more complicated system of liquid and solids (Gurioli et al. 2014; Oppenheimer et al., 2020). At Stromboli, Gurioli et al. (2014) described two quenched bombs where fresh magma was mingled with batches of degassed, oxidized, microlite-rich and evolved magma with high viscosity and crystallinity. They hypothesized that this stagnant and oxidized magma formed a rheological layer at the top of the magmatic column through which the fresh magma burst. Textural modeling and geophysical analysis confirmed that the presence of this high density, high viscosity magma layer modulates the type of emission during normal activity (e.g. Lautze et al. 2005; Leduc et al. 2015; Gaudin et al. 2017). This layer could be related to the presence of debris on top of the vent (Patrick et al., 2007; Capponi et al., 2016) and/or the presence

77 of a plug made up of cooled, degassed and partially crystallized magma at the top of the column
78 (Capponi et al., 2016; Del Bello et al., 2015; Lautze and Houghton, 2007; Oppenheimer et al., 2020;
79 Suckale et al., 2016).

80 Small and large scale paroxysms punctuate persistent activity at Stromboli on annual and
81 decadal time scales (Rosi et al., 2013). Also termed "major explosions" (Barberi et al., 1993;
82 Bertagnini et al., 1999; Harris and Ripepe, 2007b), small-scale paroxysms consist of events
83 involving 10^4-10^5 kg of material, have a duration of around a minute (Gurioli et al., 2013), and are
84 accompanied by short-lived plumes reaching a height of about 1 km (Rosi et al., 2013). They cause
85 discontinuous ballistic fallout within a distance of 500 m (Gurioli et al., 2013), and ash fall to the
86 coast (1.5 km distant) and beyond (Andronico and Pistolesi, 2010). Large scale paroxysms (Rosi et
87 al., 2013) involve 10^6-10^7 kg of material (Rosi et al., 2006) and are the most powerful eruptive
88 events recorded historically at Stromboli (Barberi et al., 1993; Bertagnini et al., 2011). They last
89 several minutes and can send meter-sized bombs and blocks up to 2 km from the craters, with the
90 concurrent formation of a convective plume that can ascend several kilometers (up to 10 km) above
91 the vents (Pistolesi et al., 2008; Rosi et al., 2013). These larger events have been explained as
92 having a deeper trigger than normal explosions. Eruptive dynamics during paroxysms is believed to
93 be controlled by ascent of a deep-seated, volatile-rich, magma that mingles with a degassed magma
94 residing in the shallow reservoir (Métrich et al., 2010).

95 Although spanning five orders of magnitude in terms of erupted mass, the small and large
96 scale paroxysms appear to be associated with the same near-surface conduit dynamics as normal
97 explosions, where the point of fragmentation is just a few 10's to 100's of meters below the vent
98 (Ripepe and Harris, 2008). For some small scale paroxysms, partial plug obstruction has been
99 observed and invoked as a trigger mechanism (Calvari et al., 2012). Calvari et al. (2014) also
100 suggested that, between 2007 and 2012, the geometry of the upper portion of the system evolved by
101 developing into a wide collapse depression that consumed the uppermost conduit, and which then
102 became refilled by partially melted hot debris and scoria (Del Moro et al., 2013). These structural

changes modified the shallow feeder conduit allowing a greater volume of magma to be stored and degas at quasi equilibrium conditions, a volume which stays hotter for longer, enhancing the possibility for the degassed magma to mingle with the deep-seated magma and increase the number of small scale paroxysms (Calvari et al. 2014).

Within this framework of current understanding of Strombolian activity, we present results from an interdisciplinary study in which we are able to texturally and chemically characterize the magma sitting at the top of the shallow conduit at Stromboli, as emitted during a small scale paroxysm that occurred on 21 January 2010. Our aim is to investigate the possible role of this magma in the formation of a plug during more energetic Strombolian (small scale paroxysms) eruptions. The work is based on complete mapping of an entire bomb-field associated with a small scale paroxysmal tied to detailed sampled to generate a unique data set of bombs, collected for the first time from a single bomb field emitted during a small scale paroxysm at Stromboli. We show that these bombs represent a window into the character of Stromboli's conduit allowing us to define the nature of the shallow magma associated with small scale paroxysms. We find that, for the small scale paroxysm sampled here, a dense and crystal-rich plug at the top of the conduit controlled the eruption style, a finding which links the genesis of small scale paroxysmal Strombolian explosions to that of normal activity.

2. Stromboli magmatic system and textural features

Stromboli volcano exhibits a wide range of explosive styles which reflect differences in the magma involved. Normal activity and effusive events are fed by a crystal-rich and volatile-poor high porphyritic (HP) magma (Bertagnini et al., 2008, 1999; Francalanci et al., 2004, 1999; Landi et al., 2008; Métrich et al., 2010, 2001). HP magma contains 45-55 vol% of plagioclase (0.1-2.5 mm), clinopyroxene (0.5-5 mm) and olivine (0.1-4 mm) in equilibrium with a shoshonitic residual melt (~52 wt % SiO_2 and ~4.5 wt% K_2O). This magma is emitted as black scoriae. Different textural facies have been described for HP scoriae associated with normal activity (Andronico et al., 2008;

129 Belien et al., 2010; Colò et al., 2010; Gurioli et al., 2014; Lautze and Houghton, 2008, 2007, 2005;
130 Leduc et al., 2015; Polacci et al., 2006) and a review of all published data is given in Table C1.
131 During large, as well as in some small scale paroxysms, in addition to HP magma, a crystal-
132 poor and volatile-rich melt is erupted, this being low porphyritic magma (LP, Table C1) (Bertagnini
133 et al., 2008, 1999; Francalanci et al., 2004, 1999; Métrich et al., 2010, 2001; Pioli et al., 2014). LP
134 magma is rarely released as pure "golden pumice" even in ash and fine lapilli size and is often
135 variably mingled with the HP magma (Pioli et al. 2014). LP magma contains the same mineral
136 phases present in HP scoriae, although plagioclase is lacking as phenocrysts. Crystallinity is also
137 lower (<5 vol%) in respect to the black scoria, and the LP groundmass glass has a basaltic
138 composition (~48 wt % SiO_2 and ~2.5 wt% K_2O) (Bertagnini et al., 1999; Francalanci et al., 2004;
139 Rosi et al., 2013).
140 Stromboli's plumbing system has become envisioned as a polybaric multi-reservoir system
141 (Métrich et al., 2010; Pichavant et al., 2011; Pompilio et al., 2012), consisting of: (i) a shallower
142 reservoir (~2 km) where the HP magma resides, (ii) a deep ponding zone at 7-10 km occupied by
143 LP magma, and (iii) a complex transition zone between the two, possibly characterized by a crystal
144 mush zone periodically influenced by ascending LP magma (Francalanci et al., 2004, 1999; ;
145 Métrich et al., 2010). With this in mind, the HP magma most likely derives from LP magma
146 through crystallization driven by decompression and water exsolution at low pressure (Métrich et al.
147 2001).
148
149 **3. The small scale paroxysm of 21 January 2010**
150
151 At 20:45:03 (local time) on 21 January 2010, thermal, infrasonic and seismic sensors of the
152 University of Florence (Italy) recorded a strong explosion at Stromboli. This small scale paroxysm
153 lasted 51 seconds, consisted of three main phases, and was described in detail by Gurioli et al.
154 (2013). The explosion occurred after few days of crater inactivity. Following the reconstruction of

Gurioli et al. (2013), Phase 1 comprised two simultaneous bursts which sent bombs to the S/SSE and SW. Each burst comprised two components: a leading spray of smaller bombs quickly followed by emission of larger bombs that attained lower heights and fell closer to the vent than those of the first burst. An associated cloud of gas and scarce finer material was observed, mostly connected to the SW-directed burst and directed at an angle of 45°. The second phase began after seven seconds and involved emission of two or three plumes of gas and scarce fine particles, lacking bombs. Phase 2 was effectively over within 20 seconds and was followed by a third phase marked by a series of weakening gas-rich puffs that lasted 24 seconds. Bombs were characterized by launch velocities between 52 and 70 m/s and the total erupted bomb mass was 3.6×10^4 kg, with bomb mass emission rates being around 2×10^4 kg s^{-1} (Gurioli et al., 2013). Fine fragments were indistinguishable and/or minimal across the deposit (only one coarse lapilli was found), and sedimentation from phases 2 and 3 produced no distinguishable layer in more distal locations, as instead was observed for the small scale paroxysm of 24 November 2009 (Andronico and Pistolesi, 2010).

4. Sampling and analytical methods

4.1 Sample collection

Samples studied in this work were mapped and collected during two sampling campaigns: one in June 2010 and another in June 2011 (6 and 18 months after the January 2010 eruption that emplaced the sampled bombs). In total, 780 bombs were mapped (Fig. 1) and 55 bombs representative of the deposit were sampled, in June 2010, along the longitudinal and horizontal dispersal axis (Fig.1, Gurioli et al., 2013) every ten meters. As explained by Gurioli et al. (2013), the thermal video of the 21 January event revealed bombs moving away from the camera, indicating a southward dispersal direction opening at an angle of 180° (Fig. 1). Within this expected landing distribution, we mapped the SSE- and the SW-directed bursts (Fig. 1). This means that the small

scale paroxysm of 21 January 2010 was the source of the bombs, because it was the only explosion of the series of six small scale paroxysms events that occurred between May 2009 and May 2010 with such a dispersal direction. This distribution was confirmed by checking of thermal video for all six small scale paroxysms that occurred during 2009-2010 (cf. Table 1 of Gurioli et al., 2013). The bomb field of 24 November 2009 had a southeast dispersion axis (Andronico and Pistolesi, 2010). This field overlaps that of 21 January 2010 to the east, but the majority of these bombs (purple diamonds in Fig. 1) can be distinguished based on their larger size and on photos taken before and after the 21 January 2010 explosion (see Item DR1, in Gurioli et al. 2013). All measured and collected bombs from the January 2010 event were fresh, glassy and iridescent, and stratigraphically above older pyroclasts—a characteristic that, even after 18 months, allowed them to be easily distinguished. Furthermore, all bombs were photographed, measured (for long and short axis) and GPS-located during the June 2010 campaign, allowing them to be relocated with confidence during the June 2011 campaign, when the dispersion map was better defined and further morphological measurements of the bombs were made.

4.2 Density and textural measurements

For the 55 bombs sampled by Gurioli et al. (2013), densities were measured both as bulk density of the entire bomb (Figs. 2A-F and Table C3 in Appendix C) and as density of the marginal portion of the bomb (including quenched rind and some portion of the bomb, see limits of the thin section areas Figs. A1 to A6 in Appendix A). Density was measured by comparing the sample weight in water with the sample weight in air. While bomb rinds were made impermeable using Parafilm™ wax, bulk bomb (which were larger than 8-10 cm) density measurements were carried out following the "natural waterproofing" strategy (Gurioli et al., 2015). We measured the weight of the bombs in water using the apparatus of Fig. 2G. The quenched rind prevented the water from entering the interior, as confirmed by the lack of bubble formation in the water and the constant weight of the bomb before and after immersion. After these measurements, bombs were cut into two slices along

207 the major axis and thin sections prepared from the marginal portions of 12 samples. Vesicularity
208 (Φ) was determined using the dense rock equivalent (DRE) density of 2850 kg/m^3, as measured by
209 Pistolesi et al. (2011).

210 Textural measurements, both for vesicles and crystals, were performed on 12 bombs
211 following the technique of Leduc et al. (2015). Images of sliced bombs and thin sections were
212 acquired using a desktop scanner, while the JEOL JSM-5910LV scanning electron microscope
213 (SEM) at Laboratorie Magmas et Volcans (LMV) in Clermont-Ferrand (France) was used for larger
214 magnification images. Each image was adjusted in Adobe Photoshop (e.g., broken bubble walls
215 were connected) and processed using the Fast Object Acquisition and Measurement System
216 (FOAMS) software of Shea et al. (2010). From each image, vesicles (black), crystals (white) and
217 glass (gray) were extracted (Fig. B1, Appendix B). Percentage of vesicles and crystals were then
218 measured (Table 1) and vesicle volume plots created (Fig. B2). Our CSD plots represent the
219 distribution of all mineral species: we assumed that plagioclase crystals dominate the
220 microphenocrysts and microlites range, while clinopyroxene and olivine crystals rule the
221 phenocrysts population (see Figure B5).

222

223 *4.3 Geochemical analysis*

224 Chemical analysis of groundmass glasses, phenocrysts and melt inclusions (MI) were carried out
225 using the Philips XL30 SEM at the Dipartimento di Scienze della Terra (DST, Università di Pisa,
226 Italy) integrated with an energy-dispersive X-ray spectroscopy (EDS) which employs the EDAX-
227 DX4 software. Operating conditions were a 20 kV voltage and a 0.1 nA beam current. A raster area
228 of 100 μm^2 was employed for glass analysis to reduce light element loss. A set of reference
229 standard of natural trachytic (CFA47), basaltic (ALV981R23) and pantelleritic (KE12) glasses was
230 analyzed before each session. Major element composition of the groundmass glasses was analyzed
231 using the electron microprobe (EMP), SX-100 CAMECA, at LMV. Operating conditions were an

accelerating voltage of 15 kV and a defocused beam with an 8 nA current intensity. A comparison between EDS and EMPA analysis is reported in Table C5.

Phenocrysts were hand-picked, mounted on slides and double polished. After petrographic inspection, selected melt inclusions were prepared for volatile measurements. H_2O and CO_2 were analyzed by transmission IR spectroscopy (FTIR) using a Nicolet iN10 equipped with a high-intensity EverGlo IR source and a MCT-A detector cooled with liquid nitrogen at DST. Concentrations were calculated according to the Beer-Lambert law: $C = Abs \times PM / \varepsilon \times \rho \times d$, where Abs is the absorbance, PM the molar mass (g/mol), ε the molar absorptivity (L/mol-cm), ρ the MI density (kg/m^3) and d the MI's thickness (cm). Melt density was calculated by major element composition (average 2630 kg/m^3) and thickness of each sample was measured using a calibrated optical microscope. All the measured and calculated Beer-Lambert parameters are given in table C2.

5. Results

5.1 Macroscopic description and density analysis

All sampled bombs are uniformly black with dimensions ranging from 5 to 44 cm, the smallest clast being the only coarse lapilli found and sampled across the bomb field (Figs. 2A to 2E and Figs. A1 to A6,). Most have a quenched rind (Figs. 2B, 2D and 2E) of variable thickness (4-18 mm) which is rich in crystals and small vesicles (e.g. S20 in Fig. A1 and A7 in Fig. A5,), while slightly larger vesicles are normally clustered, more or less homogeneously, in the interior of the bomb (Fig. 2). Occasionally, the central portion of the bomb is characterized by a large, centimetric void (Fig. 2E). The occurrence of this difference between the marginal portion and the center is more marked for the highly vesicular samples, while some of the densest bombs lack such a difference (Fig. 2 and Figs A1 to A6,). However, even in the vesiculated samples, poorly-vesiculated areas are scattered across the whole bomb surface. All bombs are scoriaceous apart from one (Fig. 3A), which contains

an elongated, light toned, vesicle-rich and crystal-poor pumice zone, typical of LP magma. The contact between the pumiceous and scoriaceous zone is sharp and well-defined near the bomb's outer edge, but irregular towards the interior (Fig. 3A).

Densities for all of the 55 samples have a Gaussian trend, with density values in the range of 1100 to 2300 kg/m^3 (Fig. 2F and Table C3). Similarly, the marginal portion samples (the cut for the thin sections) record narrower density range (1140-2050 kg/m^3). Density values for the marginal portion are always lower than the correspondent values for the whole bombs (Table 1).

5.2 Textural data

For the twelve analyzed bombs, porosity decreases as the number of large, coalesced, centimetric to millimetric vesicles decreases (Table 1 and A1-A6; Figs. 4D, 4E and 4F). In contrast, the number of small vesicles (<50 µm in diameter), which are typically rounded (Fig. 4E), increases as bomb density increases. The LP facies differs from the HP facies within the same scoria sample, mostly because of its very high vesicularity, with a population of rounded, small to medium sized vesicles that are normally organized in chains (Fig. 4C).

The simplest vesicle volume distribution histograms (VVDs, Fig. 5A-D) display unimodal, symmetrical distributions, with vesicles ranging from 0.03 to 18 mm and a mode value at around 1.8 mm. More complex VVD histograms are characterized by negative or positive asymmetrical distributions with the same modes at 1.8 mm or finer modes at 1.3 or 0.7 mm (Fig. B2). Only for A23, S20 and S28 a bimodal distributions is present due to a second coarse population around modes of 4, 7 or 17 mm (Fig. B2). VVDs for whole bombs (in black in Figs. 5A-C and B2) and marginal portions (in grey in Figs. 5A-C and B2) are very similar, although the marginal portions are always more vesicular than the corresponding whole bomb. Only the LP texture (Fig. 5D) is different, having a much greater vesicularity (67 %) and a unimodal, symmetrical distribution. This latter distribution is due to the lack of large vesicles and abundance of small vesicles with a main

mode at around 0.5 mm (Fig. 3C and Fig. 5D). In agreement with Polacci et al. (2009, 2006) and Cigolini et al. (2008), corrected vesicle number density (N_v^{corr}) values are of the order of magnitude of 10^2 and 10^3 mm^{-3}, with the LP texture having the greatest value (Table 1). Some of the densest scoria also have relatively high values of N_v^{corr} due to an increase of small vesicles in respect to the more porous scoria (Fig. 4 and Table 1).

Bombs have a crystal assemblage that comprises plagioclase, clinopyroxene and olivine (Fig. 4A) in a uniform glassy groundmass (Fig. 4B). Also in agreement with Cigolini et al. (2008) and Pioli et al. (2014), crystallinity corrected for vesicularity ranges from 30 to 63 vol. % for the scoria, but for the LP texture the crystal content is just 1.7 vol. %, (Table 1). Crystallinity is correlated with vesicularity, with the least dense bombs having the highest crystal contents (Table 1). The whole CSDs are very similar among all samples (Fig. 5E and Fig. B3-B4), where crystal sizes range from 50 μm to 14 mm. The CSD curves can be divided into three portions defined by different slopes. Based on the whole CSD population size (Fig. 5G-H and B3-B4), we defined phenocrysts as crystals with long axes of more than 350 μm, microphenocrysts with long axes between 100 and 350 μm, and microlites with long axes less than 100 μm; where microlites and microphenocrystals are mostly formed by plagioclase.

5.3 Groundmass glass and mineral chemistry

At the microscale (thin section), the groundmass glass of scoriae appears dark or light brown, although different colors do not correspond to differences in chemical composition, as already proved by Leduc et al. (2015). The chemical homogeneity of the glass is apparent in the major element oxide frequency diagrams (Figs. 6 and 8A-B). The glass is basaltic trachyandesite (SiO_2 ~ 53 wt% and CaO/Al_2O_3 ~ 0.49) with a shoshonitic character (K_2O > 4 wt%) and its SiO_2 content overlaps the bulk rock composition (Fig. 6B). Pumice glass is trachybasaltic in composition (SiO_2 ~49 wt% and CaO/Al_2O_3 ~0.61) and is distinguishable from scoria glass for MgO, FeO, TiO_2, Al_2O_3 and K_2O contents (Figs. 3B and 6). The groundmass glass has a maximum H_2O content of

1600 ppm. The bulk rock composition of the bombs falls in the trachybasalt field (white star in Fig. 6A).

Plagioclase crystals show both homogeneous and zoned textures and they are in the range An_{61} - An_{83}. Zoned plagioclases have sieved texture zones, with an An-rich cores (An_{83}) surrounded by labradoritic rims. Unzoned plagioclases are in the range An_{61-70}. Pyroxene phenocrysts, normally zoned, have diopsitic/augitic compositions, being in the range $Mg\#_{73-89}$. Olivine crystals are homogeneous and exhibit a narrow compositional range (Fo_{70-73}).

5.4 Melt inclusions: petrography, major element and volatile composition

Naturally-quenched, light brown, melt inclusions are widespread in plagioclase, olivine and clinopyroxene crystals (Fig. 7). Plagioclase crystals contain small MIs which have been neglected in our study due to their small size. Olivine and clinopyroxene crystals contain both small-sized (10-20 µm) and large-sized (>100 µm) MIs. The latter are mostly found in olivine crystals and they are usually glassy without significant petrographic evidence of post-entrapment crystallization (Fig. 7A). However, diffusive re-equilibration of the inclusion with its host can modify the composition of the trapped melt, along with crystallization of olivine on the walls of the inclusion. Therefore, we corrected olivine-hosted MI compositions for post-entrapment processes (PEP) using Petrolog 3.0. Olivine-hosted MIs required PEP correction between 0-5%. Clinopyroxene-hosted MIs needed up to 16% post-entrapment dissolution of the host mineral back into the inclusion (Table C4). A selection of raw and PEP-corrected MI compositions is reported in table C4. PEP-corrected MIs, which are used in the subsequent discussion, are chemically homogenous and they exhibit a shoshonitic character (Fig. 6), with a Na_2O+K_2O around 7.5 wt%, overlapping the groundmass field. Indeed, frequency histograms of major oxides (Fig. 8) highlight similar compositions for both MIs and groundmass glasses, showing a modal value of oxides (e.g. K_2O and FeO) centered at the same percentage. H_2O in MI ranges from 0.27-0.47 wt % (Table 2), while CO_2 content is below the detection limit.

All of our data highlight a homogeneous chemical composition, with MgO between 2.8 and 5.8 wt% and K_2O/Na_2O in the range 0.9-1.8 (Table 2), and fall within the HP glass field for normal activity (Fig. 6B) (Leduc et al., 2015; Métrich et al., 2005; Pioli et al., 2014). Only the pumice groundmass glass moves away from HP field (Fig. 3). A relation between MI and groundmass glass both in HP (and LP) products is reported in Figure 6B, as a CaO/Al_2O_3 vs K_2O diagram. MIs show a CaO/Al_2O_3 ratio around 0.40-0.60 and they plot in a field far away from MI from pumice of Pioli et al. (2014) and Métrich et al. (2001; 2005). MIs, found in pumice clasts, display more primitive features and they have a wide range of CaO/Al_2O_3, this being from 0.5 to up 1.0 (Fig. 6B).

Scoria bulk-rock chemistry is comparable with the pumice groundmass glass (Fig. 6), whereas the scoriae groundmass can be derived from the whole rock composition by crystallizing ~55 wt% plagioclase, clinopyroxene and olivine (Métrich et al., 2001), in accordance with our textural analysis (Table 1). All of these points suggest that the trapped melt (i.e. MIs) can be assumed as representative of the melt present in the conduit just before the explosion. Therefore, the volatile (H_2O and CO_2) content can be used to infer the depth of the melt in the conduit. Using VolatileCalc 2.0 (Newman and Lowenstern, 2002), we have estimated a minimum volatile saturation pressure of 13.5 MPa. This estimated pressure, assuming a magma DRE of 2850 kg/m^3 (Pistolesi et al., 2011) , corresponds to a depth of about 480 m.

6. Discussion

6.1 Textural evidence for a degassed magma

The marginal portions of the bombs have lower density values with respect to their parental bomb. Usually this should be the inverse, because the external portions of a bomb should be quenched faster than the internal portion and preserve a pristine texture where expansion and coalescence of vesicles are impended. In contrast, vesiculation (in terms of expansion and/or coalescence) and sometimes crystallization, in the bomb interior, continues after emission, so processes of post-

362 deposition modification are prevalent (e.g., Fig. 2E). Therefore, post-fragmentation expansion and
363 formation of blisters at the center of a bomb should reduce the density values for the whole bomb
364 over those of the quenched surface. In our sample collection, only a few bombs have large gas
365 blisters (Figure 2E), but those quantified in this study (see photos in Appendix A) are not as
366 expanded as they should have been because we are dealing with gas-depleted magma. Only in a few
367 bombs can we see concentration of large vesicles, but we see no real vesicle gradient (samples S27,
368 S20, A25, A7). The lack of a any obvious expansion gradient, the lack of large vesicles and the
369 presence of scattered, less vesiculated areas, causes the whole bomb to be denser than the area
370 covered by the thin section. However, all bombs, even those with central blisters, belong to the high
371 density (HD) class described by Lautze and Houghton (2005) and have densities comparable with
372 the highest values found by Gurioli et al. (2014) (Table C1). This means that these products are
373 truly degassed, so that the internal vesicles could not have expanded to any significant extent.
374 Generally, at Stromboli, post fragmentation expansion features are more predominant in the scoria
375 lapilli grain size (which are slightly richer in gas in respect to bombs), resulting in an increase in
376 clast density as the size of the pyroclast increases (see Fig. 1 in Bombrun et al. 2015).
377 Low density material was not found across the bomb field (Gurioli et al. 2013) and there
378 was no evidence of distal sedimentation of fine material, as observed by Andronico and Pistolesi
379 (2010) for a small scale paroxysm at Stromboli in 2009. The degassed nature of the magma is borne
380 out by MI data, which suggests the occurrence of a degassed magma residing in the shallow system.
381 However, this magma (Fig. 6B) is not as microlite-rich and is not as evolved as the magma found
382 by Gurioli et al (2014). As explained by Gurioli et al (2014), bombs sampled during normal activity
383 undergo cooling, crystallization and oxidation because sit at the very top of the magmatic column,
384 being a thin rind at the free surface and therefore representing a very thin crust at the head of the
385 degassing magma column. In the 2010 small scale paroxysm sampled here, we did not find the
386 equivalent of such a thin conduit-capping “crust”. Based on our observations of the thermal video
387 for the 2010 event, we argue that this crust probably fell within 200 m of the vent where it was not

388 possible to sample. However, the degassed magma within the conduit, that was resident beneath the
389 cooling crust, was too hot to crystallize microlites or to undergo oxidation, although the zonation of
390 the plagioclase reveals a prolonged residence time within the shallow conduit (cf. Landi et al.,
391 2004), as does the reduction in vesicles in the high density products. This is also clear in Figure 2
392 where low density bombs are associated with post-eruption vesicular gradients, which it is not the
393 case for high-density samples (Figs. 2b, 2d and 2e). These high-density bombs thus represent the
394 physical characteristics of the magma at the top of the column at the moment of the explosion.
395 VVDs are generally used to infer the condition of the bubbles in the magma at the time of
396 explosion if quenching is effective and post fragmentation can be excluded (Gurioli et al. 2018,
397 2015, 2014; Polacci et al. 2006). The single mode observed here is consistent with a single bubble
398 nucleation and growth event, while bimodal distributions have been observed only in the three
399 samples having the best evidenced of expansions and coalescence for the large vesicles. While large
400 vesicles dominate in relatively low-density bombs, small vesicles increase in number in the high-
401 density products, where coalescence is less visible. These features are consistent with Lautze et al.
402 (2008, 2007, 2005) and Gurioli et al. (2014) who found that the most outgassed material, which
403 experiences a longer residence time in the conduit relative to the traditional HP magma, was denser
404 and lacked syn-eruptive coalescence signatures. Following Belien et al. (2010), we can also ascribe
405 the presence of small-sized vesicles as being due to the influence of crystals. Crystal content is
406 positively correlated with the percentage of small-sized vesicles, where bubbles will deform and
407 split during percolation processes occurring in a steadily crystalizing mixture. All of these
408 observations indicate that the erupted bomb mass derived from a slowly degassing, crystallizing
409 source sitting at the top of the shallow system. Although emitted as part of a small scale paroxysm,
410 the texture of the bombs suggests a single stage of bubble nucleation and growth, typical of normal
411 Strombolian activity (cf. Lautze and Houghton, 2005; Polacci et al., 2006).
412 CSDs show similar relationships to those presented by Pioli et al. (2014). In Figure 5F we
413 plot CSD curves with the highest (black) and lowest (grey) crystallinities from Pioli et al. (2014),

414 Fornaciai et al. (2009) and this study. While normal activity samples (Fornaciai et al. 2009) show
415 linear trends, samples emitted during small scale paroxysms appear to correlate with crystallinity,
416 with low crystal frequencies at lower crystallinities, as also found by Pioli et al. (2014). Finally, the
417 small size interval of CSD curves can be affected by crystal fragmentation (Forien et al., 2011)
418 which would produce the observed exponential trends.
419
420 6.2 *Geochemical constraints and volatile-based estimates*
421 Our chemical data highlight the exclusive occurrence of a shoshonitic, chemically
422 homogeneous (HP) magma. Only the pumice groundmass glass moves away from the HP field and
423 its chemistry is consistent with a deep-seated LP magma as defined by Métrich et al. (2010). A
424 distinction between HP and LP glass is clearly shown in Figure 3B, where we report a geochemical
425 transect across the HP-LP-HP facies. The two melts are distinguishable especially at the edge
426 between the scoria and the pumice, where the LP glass has a more primitive signature. The
427 observed gap between the composition of pumice and of scoria glass, together with the element
428 frequency diagrams (Fig. 8), allow us to rule out mingling processes down to a micrometric scale.
429 Therefore we interpret the "golden pumice" as a xenolith that was present at the top of the
430 magmatic column before the explosion, which was emitted during an earlier event and then
431 recycled by the sampled event. Many bombs were also broken in the field and did not show
432 evidence of LP portions. Nevertheless, the LP magma presence cannot be totally excluded, as we
433 could not sample the very scarce finer material visible in the explosions. Evidence of LP magma in
434 coarse ash from normal activity has already been well documented by D'Oriano et al. (2011). Thus,
435 this small scale paroxysm appears to have involved, and been driven by, an entirely HP magma.
436 The low volatile content of our glasses is consistent with a magma that has been free to
437 degas, and which has thus lost almost all of its H_2O and CO_2. From MI investigations we can thus
438 assume that MIs were trapped inside the shallow portion of the conduit above a depth of 500 m.
439 This depth corresponds at the zone where very long period (VLP) signals have been located during

normal through paroxysmal activity at Stromboli (Chouet et al., 2003; Ripepe and Harris, 2008; Gurioli et al., 2014), reinforcing the MI-based pressure calculation and increasing the strength of the argument posed by our data. We note, here, that the depth of the VLP has not been linked to the thickness of any degassed layers, but instead has been related to a level at which gas coalescence may occur (Ripepe et al. 2001; Chouet et al. 2003), at which a specific conduit geometry exists that promotes a change to a bubbly flow regime (James et al. 2009), or where the last crystallization may occur, as shown in this paper. Instead, considering the total mass of the deposit of 3.6×10^4 kg (Gurioli et al., 2013) and a mean bomb bulk density of 1850 kg/m^3, for a conduit diameter of 1 m (Vergniolle et al., 1996), we can estimate the in-conduit thickness of the erupted, degassed HP magma to have been approximately 25 m, in agreement with the length of the plug of 10-50 m estimated by Woitischek et al. (2020). This would thus have contributed a 25 m thick layer at the head of a density-stratified magma column above the VLP, with our data suggesting that crystallization is complete (or completed) by the depth of the VLP.

6.3 Implication for Strombolian eruptions

The homogeneous nature of these bombs is in contrast with the hypothesis of a finger-like system composed of a network of smaller volumes of different magma, as proposed in Calvari et al (2014). In such a scenario we should have expected a more heterogeneous deposit with evidence of non-juvenile materials stripped off from the explosion and mingling with the LP magma. The presence of the LP magma involved as xenoliths can be consistent with a simpler, large storage reservoir that allows more HP magma to accumulate and at the same time, preserve old magma left behind by more energetic explosions.

Oppenheimer et al. (2020) investigated and modelled the physical interactions between bubbles and crystals defining a “soft plug model” for Strombolian eruptions, in which large quantities of crystals temporally impede and/or delay bubble ascent, with consequent bubble accumulation under the plug increasing until the pressure exerted by this building accumulation

becomes suddenly released. The term “soft” is used for this kind of low-melt-viscosity plugs, that areequivalent to the rheologically “stronger” plugs involved in Vulcanian-style eruptions (cf. Oppenheimer et al., 2020). It is known that magma residing in the shallow conduit of Strombolian volcanoes are crystal rich, with 30 to 60 vol%. This amount of crystals is responsible for the development of an effective yield strength which favors bubble accumulation and subsequent local overpressure. We believe that the 21 January 2010 small scale paroxysm at Stromboli volcano is consistent with the fragmentation of a dense and crystallized plug of magma residing in the upper part of the conduit. Fragmentation of this 25 m thick plug resulted in the generation of a very coarse population of pyroclasts that ascended the conduit and fed the resulting plume.

Our study thus shows that a “soft” plug control exists for Strombolian explosions, where eruptive events involve crystal-rich magmas which form strong and poorly-permeable plugs (Oppenheimer et al., 2020) through which ascending slugs must burst during both normal and paroxysmal eruptions (cf. Gurioli et al., 2014). Possibly, for the small scale paroxysms, the change in geometry of the upper feeding systems could have favored the accumulation of a relatively large quantity of HP magma (Calvari et al. 2014). We here show that, in addition to the configuration of the flow within the conduit (Capponi et al., 2016; Del Bello et al., 2015; Oppenheimer et al., 2020; Suckale et al., 2016), the transition between different strombolian activity styles is controlled by the presence of a crystal-supported stagnant magma sitting at the top of the magma column. This suggests that a weak plug model is reasonable for “strombolian” systems characterized by moderate-to-high crystallinities, as also observed for other strombolian-type eruptions such at Yasur, Villarrica and Erebus volcano (Woitischek et al. 2020).

7. Conclusion

Recent work has shown that the shallow system at Stromboli is a highly dynamic environment (Calvari et al. 2014) that experiences a continual change in the character and rheology of the resident magma during normal explosive activity (D’Oriano et al., 2011; Lautze and Houghton,

2008, 2007; Leduc et al., 2015). In this model, a degassed layer with high viscosity and yield strength (Gurioli et al., 2014), or a "plug" (Calvari et al., 2012; Oppenheimer et al., 2020; Suckale et al., 2016), can form and decay (Leduc et al., 2015). Suckale et al. (2016) argued for the presence of a porous plug of HP magma beneath the entire crater terrace, made up of crystals, bubbles and melt, but with an overall solid-like behavior. In this interpretation, normal eruptions are connected to the tensile failure of the plug due to over-pressurization following build up, or arrival, of gas volumes at the base or within the plug; failure of the plug then feeds the eruption during normal events (Gurioli et al., 2014). Our data now indicate that some small scale paroxysms have a similar genesis, meaning that the model, and process, scales-up.

Large, and some of the small, paroxysmal events at Stromboli have typically been considered as associated with the ascent of deep-sourced LP magma (Andronico and Pistolesi, 2010; Cigolini et al., 2015; Pistolesi et al., 2011). However, bombs sampled from the 21 January 2010 small scale paroxysm show that this is not the case. Indeed, we find that no LP magma was involved, and that the emission resulted from the fragmentation of a cap of degassed and dense HP magma. Thus, the capping model invoked for normal explosions at Stromboli can be scaled up to small scale paroxysms with a deformed flow regime (Oppenheimer et al., 2020) governing the ascent dynamic. In the case of the small scale paroxysm examined here, the higher magnitude and energy (and thus also distance reached by the bombs) is due to the formation of a plug when compared with normal explosions. The period of inactivity at the crater involved (a few days) probably allowed the plug to form a cold crust, obstructing the crater and promoting a larger explosion than normal. This finding strongly supports that we need to review our mechanical model for Strombolian eruptions and move away from simple foam collapse and bubble ascent speed models (e.g., Parfitt, 2004) in rheologically "clean" and simple conduits, and move towards more complex models (Del Bello et al., 2015; Oppenheimer et al., 2020) which consider strong rheological stratification effects due to near-surface crystallization processes. Our findings thus support a new model whereby shallow conduit dynamics control the magnitude, intensity and

518 character of Strombolian explosions, even the more explosive events, where for all cases the effect
519 of a degassed, crystallized cap must be considered.

Acknowledgments

520 This research was financed by the French Government Laboratory of Excellence initiative n
521 XXANR-10-LABX-0006, the Région Auvergne, and the European Regional. This work was also
522 supported by the University of Pisa 2016 Ateneo funds and by the Erasmus + traineeship funding
523 program from Pisa University (Italy).We are thankful to Jean-Luc Devidal for assistance with
524 EMPA analyses at LMV and to Franco Colarieti for help with sample preparation at DST. We are
525 very grateful to Heather Handley for the editorial handling and we thank two anonymous reviewers
526 for their constructive suggestion that improved the quality of the manuscript.

Figure captions

527 **Figure 1**. Slope map of the summit crater area of Stromboli showing the location of mapped and
528 sampled bombs. Bombs studied in this work are shown in red. Inset: location map of Stromboli in
529 the Tyrrhenian sea.

530 **Figure 2**. Bomb slices of different size and density from the 21 January 2010 small scale paroxysm
531 at Stromboli. A) and C) Dense bombs without a quenched rind and with random vesicles
532 distribution; B) and D) Lighter bombs with a quenched marginal portions and a vesicularity
533 gradient; E) Bomb with a thick quenched rind and a large central vesicle, like a blister. F) Bulk
534 densities analysis of the 55 sampled bombs reported in a density vs sample frequency diagram. G)
535 Technique used to measure the bombs density. Samples were weighed considering a natural
536 waterproofing (Gurioli et al., 2015), measuring the weight before and after the immersion. No
537 weight changes have been measured on these values. ρ: bomb density

538 **Figure 3.** A.I) Bomb A25 containing an elongated golden pumice (red square). A.II) thin section
539 image of the pumice where it is specified the position of the chemical transect (dashed red line).
540 A.III) Electron back-scattered (BSE) image of the sharp contact (red line) between the HP magma
541 and the LP magma. B) Geochemical transect across the HP-LP-HP magma in a diagram distance
542 (μm) vs TiO_2 concentration. The two distinct melts are clear distinguishable especially at the edge
543 between the scoria and the pumice. This chemical distinction is also observed with other oxides as
544 MgO, FeO and Al_2O_3.

545 **Figure 4.** Textural characteristics of the products from the 21 January 2010 small scale paroxysm at
546 Stromboli. A) Microscope image at polarized light showing the general mineral assemblage formed
547 by plagioclase, pyroxene and olivine. B) BSE image of the groundmass glass (light grey); in darker
548 grey are the plagioclase and in black the vesicles; C), BSE-SEM image of the vesicle-rich golden
549 pumice; D), E) and F) BSE images of scoria with different vesicularity.

550 **Figure 5.** Vesicle volume distributions (VVDs) and crystal size distribution (CSDs) for selected
551 samples. (A-C) VVDs for three selected scoria samples and (D) for the golden pumice in sample
552 A25. Each diagram is formed by a grey histogram (representative the texture of the marginal
553 portions of the bombs) and a black histogram (representative the texture of the whole bomb). The
554 golden pumice is in white and the distribution is characterized by a predominance of small-size
555 vesicles. For each sample, we indicate the vesicularity of the whole bomb (Φ_{bomb}) and of the
556 marginal portions (Φ_{quen}). (E) CSDs of all studied samples, in the crystal size interval 0-15mm.
557 Single CSD curves are reported in appendix B3 and B4. (F) CSDs of samples with the highest and
558 lowest crystallinity from this study and comparison with samples studied in Pioli et al. (2014) and
559 Fornaciai et al. (2009). (G-H) CSD curves in a restricted crystal size range (0-1.4 mm), showing the
560 three crystals families (gray lines), as microlites (<100μm), microphenocrystals (100-350 μm) and
561 phenocrystals (>350 μm).

562 **Figure 6.** Scoria groundmass glass analyses (red circles) and olivine- and pyroxene-hosted melt
563 inclusions (orange triangles) of scoria samples and pumice groundmass glass (yellow circles)

564 plotted in A) a TAS diagram and in B) CaO/Al_2O_3 vs K_2O/Na_2O diagram. Both groundmass glasses
565 and MI from scoriae show a shoshonitic composition. In the CaO/Al_2O_3 vs K_2O plot MIs and
566 glasses cluster in the Stromboli HP field. *LP and HP field of Stromboli MIs and groundmass
567 glasses are represented accordingly to Métrich et al. (2005, 2001) and Pioli et al. (2014). For
568 comparison, we also report the more evolved groundmass glass compositions (gray circles) found
569 by Gurioli et al. (2014).

570 **Figure 7.** (A-B) Transmission microscope images of naturally-quenched olivine-hosted melt
571 inclusions; (C-F) back scattered images of significant large-size MIs. MIs are glassy and fully
572 enclosed, without any significant post-entrapment transformation. For each olivine crystal we
573 indicate the forsterite (Fo) content. Cpx: clinopyroxene crystal included in the melt inclusion.

574 **Figure 8.** Variation histograms for FeO and K_2O in (A-B) groundmass glasses and (C-D) melt
575 inclusions. Histograms are unimodal and for each oxide we observe a main mode fixed at the same
576 value. This variation is also observed in term of MgO, FeO, Al_2O_3 and K_2O.

References

577 Andronico, D., Corsaro, R.A., Cristaldi, A., Polacci, M., 2008. Characterizing high energy
578 explosive eruptions at Stromboli volcano using multidisciplinary data: An example from the 9
579 January 2005 explosion. J. Volcanol. Geotherm. Res. 176, 541–550.
580 https://doi.org/10.1016/j.jvolgeores.2008.05.011

581 Andronico, D., Pistolesi, M., 2010. The November 2009 paroxysmal explosions at Stromboli. J.
582 Volcanol. Geotherm. Res. 196, 120–125. https://doi.org/10.1016/j.jvolgeores.2010.06.005

583 Barberi, F., Rosi, M., Sodi, A., 1993. Volcanic hazard assessment at Stromboli based on review of
584 historical data. Bull. Volcanol. 3, 173–187.

585 Belien, I.B., Cashman, K. V., Rempel, A.W., 2010. Gas accumulation in particle-rich suspensions
586 and implications for bubble populations in crystal-rich magma. Earth Planet. Sci. Lett. 297,
587 133–140. https://doi.org/10.1016/j.epsl.2010.06.014

588 Bertagnini, A., Coltelli, M., Landi, P., Pompilio, M., Rosi, M., 1999. Violent explosions yield new
589 insights into dynamics of Stromboli volcano. Eos (Washington. DC). 80, 2–8.
590 https://doi.org/10.1029/99EO00415

591 Bertagnini, A., Di Roberto, A., Pompilio, M., 2011. Paroxysmal activity at Stromboli: Lessons from
592 the past. Bull. Volcanol. 73, 1229–1243. https://doi.org/10.1007/s00445-011-0470-3

593 Bertagnini, A., Métrich, N., Francalanci, L., P., L., Tommasini S., Conticelli, S., 2008. Volcanology
594 and magma geochemistry of the present-day activity: constraints on the feeding system. In:
595 Calvari, S. Inguaggiato, S., Puglisi, G., Ripepe, M. Rosi, M. (Eds.), Learming from Stromboli:
596 American Geophysical Union. Geophys. Monogr. 182, 19–38.
597 https://doi.org/10.1029/182GM04

598 Bombrun, M., Harris, A.J.L., Gurioli, L., Battaglia, J., Barra, V., 2015. Anatomy of a Strombolian
599 eruption: Inferences from particle data recorded with thermal video Maxime. J. Geophys. Res.
600 Solid Earth Res. 120, 2367–2387. https://doi.org/10.1002/2014JB011556.Received

601 Calvari, S., Bonaccorso, A., Madonia, P., Neri, M., Liuzzo, M., Salerno, G., Behncke, B.,
602 Caltabiano, T., Cristaldi, A., Giuffrida, G., La Spina, A., Marotta, E., Ricci, T., Spampinato,
603 L., 2014. Major eruptive style changes induced by structural modifications of a shallow
604 conduit system: the 2007–2012 Stromboli case. Bull Volcanol (2014) 76:841 DOI
605 10.1007/s00445-014-0841-7

606 Calvari, S., Bttner, R., Cristaldi, A., Dellino, P., Giudicepietro, F., Orazi, M., Peluso, R.,
607 Spampinato, L., Zimanowski, B., Boschi, E., 2012. The 7 September 2008 Vulcanian
608 explosion at Stromboli volcano: Multiparametric characterization of the event and
609 quantification of the ejecta. J. Geophys. Res. Solid Earth 117, 1–17.
610 https://doi.org/10.1029/2011JB009048

611 Calvari, S., Inguaggiato, S., Puglisi, G., Ripepe, M., Rosi, M., 2008. The Stromboli Volcano: An
612 integrated study of the 2002-2003 eruption. John Wiley & Sons.

613 https://doi.org/10.1029/GM182

614 Capponi, A., James, M.R., Lane, S.J., 2016. Gas slug ascent in a stratified magma: Implications of
615 flow organisation and instability for Strombolian eruption dynamics. Earth Planet. Sci. Lett.
616 435, 159–170. https://doi.org/10.1016/j.epsl.2015.12.028

617 Chouet, B., Dawson, P., Ohminato, T., Martini, M., Saccorotti, G., Giudicepietro, F., De Luca, G.,
618 Milana, G., Scarpa, R., 2003. Source mechanisms of explosions at Stromboli Volcano, Italy,
619 determined from moment-tensor inversions of very-long-period data. J. Geophys. Res. Solid
620 Earth 108, ESE 7-1-ESE 7-25. https://doi.org/10.1029/2002JB001919

621 Cigolini, C., Laiolo, M., Bertolino, S., 2008. Probing Stromboli volcano from the mantle to
622 paroxysmal eruptions. Geol. Soc. London, Spec. Publ. 304, 33–70.
623 https://doi.org/10.1144/SP304.3

624 Cigolini, C., Laiolo, M., Coppola, D., 2015. Revisiting the last major eruptions at Stromboli
625 volcano: inferences on the role of volatiles during magma storage and decompression. Geol.
626 Soc. Spec. Publ. 410, 143–177. https://doi.org/10.1144/SP410.3

627 Colò, L., Ripepe, M., Baker, D.R., Polacci, M., 2010. Magma vesiculation and infrasonic activity at
628 Stromboli open conduit volcano. Earth Planet. Sci. Lett. 292, 274–280.
629 https://doi.org/10.1016/j.epsl.2010.01.018

630 D'Oriano, C., Bertagnini, A., Pompilio, M., 2011. Ash erupted during normal activity at Stromboli
631 (Aeolian Islands, Italy) raises questions on how the feeding system works. Bull. Volcanol. 73,
632 471–477. https://doi.org/10.1007/s00445-010-0425-0

633 Del Bello, E., Lane, S.J., James, M.R., Llewellin, E.W., Taddeucci, J., Scarlato, P., Capponi, A.,
634 2015. Viscous plugging can enhance and modulate explosivity of strombolian eruptions. Earth
635 Planet. Sci. Lett. 423, 210–218. https://doi.org/10.1016/j.epsl.2015.04.034

636 Del Moro, S., Renzulli, A., Landi, P., La Felice, S., Rosi, M., 2013. Unusual lapilli tuff ejecta
637 erupted at Stromboli during the 15 March 2007 explosion shed light on the nature and thermal

state of rocks forming the crater system of the volcano. J. Volcanol. Geotherm. Res. 254, 37–52. https://doi.org/10.1016/j.jvolgeores.2012.12.017

Forien, M., Arbaret, L., Burgisser, A., Champallier, R., 2011. Experimental constrains on shear-induced crystal breakage in magmas. J. Geophys. Res. Solid Earth 116, 1–21. https://doi.org/10.1029/2010JB008026

Francalanci, L., Tommasini, S., Conticelli, S., 2004. The volcanic activity of Stromboli in the 1906-1998 AD period: Mineralogical, geochemical and isotope data relevant to the understanding of the plumbing system. J. Volcanol. Geotherm. Res. 131, 179–211. https://doi.org/10.1016/S0377-0273(03)00362-7

Francalanci, L., Tommasini, S., Conticelli, S., Davies, G.R., 1999. Sr isotope evidence for short magma residence time for the 20th century activity at Stromboli volcano, Italy. Earth Planet. Sci. Lett. 167, 61–69. https://doi.org/10.1016/S0012-821X(99)00013-8

Gaudin, D., Taddeucci, J., Scarlato, P., Del Bello, E., Ricci, T., Orr, T., Houghton, B.F., Harris, A.J.L., Rao, S., Bucci, A., 2017. Integrating puffing and explosions in a general scheme for Strombolian-style activity. J. Geophys. Res. Solid Earth 122, 1860–1875. https://doi.org/10.1002/2016JB013707

Gurioli, L., Andronico, D., Bachelery, P., Balcone-Boissard, H., Battaglia, J., Boudon, G., Burgisser, A., Burton, M.R., Cashman, K. V., Cichy, S., Cioni, R., Di Muro, A., Dominguez, L., D'Oriano, C., Druitt, T., Harris, A.J.L., Hort, M., Kelfoun, K., Komorowski, J.C., Kueppers, U., Le Pennec, J.L., Menand, T., Paris, R., Pioli, L., Pistolesi, M., Polacci, M., Pompilio, M., Ripepe, M., Roche, O., Rose-Koga, E.F., Rust, A., Schiavi, F., Scharff, L., Sulpizio, R., Taddeucci, J., Thordarson, T., 2015. MeMoVolc consensual document: a review of cross-disciplinary approaches to characterizing small explosive magmatic eruptions. Bull. Volcanol. 77. https://doi.org/10.1007/s00445-015-0935-x

Gurioli, L., Colò, L., Bollasina, Harris, A.J.L., Whittington, A., Ripepe, M., 2014. Dynamics of

Strombolian explosions: inferences from field and laboratory studies of erupted bombs from stromboli volcano. J. Geophys. Res. Solid Earth 645–660. https://doi.org/10.1002/2013JB010264.Received

Gurioli, L., Harris, A.J.L., Colò, L., Bernard, J., Favalli, M., Ripepe, M., Andronico, D., 2013. Classification, landing distribution, and associated flight parameters for a bomb field emplaced during a single major explosion at Stromboli, Italy. Geology 41, 559–562. https://doi.org/10.1130/G33967.1

Harris, A.J.L., Delle Donne, D., Dehn, J., Ripepe, M., Worden, A.K., 2013. Volcanic plume and bomb field masses from thermal infrared camera imagery. Earth Planet. Sci. Lett. 365, 77–85. https://doi.org/10.1016/j.epsl.2013.01.004

Harris, A.J.L., Ripepe, M., 2007a. Temperature and dynamics of degassing at Stromboli. J. Geophys. Res. Solid Earth 112, 1–18. https://doi.org/10.1029/2006JB004393

Harris, A.J.L., Ripepe, M., 2007b. Synergy of multiple geophysical approaches to unravel explosive eruption conduit and source dynamics−a case study from Stromboli. Geochem 67, 1-35. https://doi.org/10.1016/j.chemer.2007.01.003

Houghton, B.F., Taddeucci, J., Andronico, D., Gonnermann, H.M., Pistolesi, M., Patrick, M.R., Orr, T.R., Swanson, D.A., Edmonds, M., Gaudin, D., Carey, R.J., Scarlato, P., 2016. Stronger or longer: Discriminating between Hawaiian and Strombolian eruption styles. Geology 44, 163–166. https://doi.org/10.1130/G37423.1James, M.R., Lane, S.J., Wilson, L., Corder, S.B., 2009. Degassing at low magma-viscosity volcanoes: Quantifying the transition between passive bubble-burst and Strombolian eruption. J. Volcanol. Geotherm. Res. 180, 81–88. https://doi.org/10.1016/j.jvolgeores.2008.09.002

Jaupart, C., Vergniolle, S., 1989. The generation and collapse of a foam layer at the roof of a basaltic magma chamber, Journal of Fluid Mechanics. https://doi.org/10.1017/S0022112089001497

688 Landi, P., Métrich, N., Bertagnini, A., Rosi, M., 2008. Recycling and “re-hydration” of degassed
689 magma inducing transient dissolution/crystallization events at Stromboli (Italy). J. Volcanol.
690 Geotherm. Res. 174, 325–336. https://doi.org/10.1016/j.jvolgeores.2008.02.013

691 Landi, P., Métrich, N., Bertagnini, A., Rosi, M., 2004. Dynamics of magma mixing and degassing
692 recorded in plagioclase at Stromboli (Aeolian Archipelago, Italy). Contrib. to Mineral. Petrol.
693 147, 213–227. https://doi.org/10.1007/s00410-004-0555-5

694 Lautze, N.C., Houghton, B.F., 2008. Single explosions at Stromboli in 2002: Use of clast
695 microtextures to map physical diversity across a fragmentation zone. J. Volcanol. Geotherm.
696 Res. 170, 262–268. https://doi.org/10.1016/j.jvolgeores.2007.10.011

697 Lautze, N.C., Houghton, B.F., 2007. Linking variable explosion style and magma textures during
698 2002 at Stromboli volcano, Italy. Bull. Volcanol. 69, 445–460. https://doi.org/10.1007/s00445-
699 006-0086-1

700 Lautze, N.C., Houghton, B.F., 2005. Physical mingling of magma and complex eruption dynamics
701 in the shallow conduit at Stromboli volcano, Italy. Geology 33, 425–428.
702 https://doi.org/10.1130/G21325.1

703 Leduc, L., Gurioli, L., Harris, A.J.L., Colò, L., Rose-Koga, E.F., 2015. Types and mechanisms of
704 strombolian explosions: characterization of a gas-dominated explosion at Stromboli. Bull.
705 Volcanol. 77. https://doi.org/10.1007/s00445-014-0888-5

706 Marsh, B.D., 1981. On the crystallinity, probability of occurrence, and rheology of lava and magma.
707 Contrib. to Mineral. Petrol. 78, 85–98. https://doi.org/10.1007/BF00371146

708 Métrich, N., Bertagnini, A., Di Muro, A., 2010. Conditions of magma storage, degassing and ascent
709 at Stromboli: New insights into the volcano plumbing system with inferences on the eruptive
710 dynamics. J. Petrol. 51, 603–626. https://doi.org/10.1093/petrology/egp083

711 Métrich, N., Bertagnini, A., Landi, P., Rosi, M., 2001. Crystallization driven by decompression and
712 water loss at Stromboli volcano (Aeolian Islands, Italy). J. Petrol. 42, 1471–1490.

https://doi.org/10.1093/petrology/42.8.1471

Métrich, N., Bertagnini, A., Landi, P., Rosi, M., Belhadj, O., 2005. Triggering mechanism at the origin of paroxysms at Stromboli (Aeolian Archipelago, Italy): The 5 April 2003 eruption. Geophys. Res. Lett. 32, 1–4. https://doi.org/10.1029/2004GL022257

Newman, S., Lowenstern, J.B., 2002. Volatile Calc : a silicate melt – H2O – CO2 solution model written in Visual Basic for excel. Comput. Geosci. 28, 597–604. https://doi.org/doi:10.1016/S0098-3004(01)00081-4

Oppenheimer, J., Capponi, A., Cashman, K. V., Lane, S.J., Rust, A.C., James, M.R., 2020. Analogue experiments on the rise of large bubbles through a solids-rich suspension: A "weak plug" model for Strombolian eruptions. Earth Planet. Sci. Lett. 531, 115931. https://doi.org/10.1016/j.epsl.2019.115931

Parfitt, E.A., 2004. A discussion of the mechanisms of explosive basaltic eruptions. J. Volcanol. Geotherm. Res. 134, 77–107. https://doi.org/10.1016/j.jvolgeores.2004.01.002

Patrick, M.R., Harris, A.J.L., Ripepe, M., Dehn, J., Rothery, D.A., Calvari, S., 2007. Strombolian explosive styles and source conditions: Insights from thermal (FLIR) video. Bull. Volcanol. 69, 769–784. https://doi.org/10.1007/s00445-006-0107-0

Pering, T.D., McGonigle, A.J.S., James, M.R., Tamburello, G., Aiuppa, A., Delle Donne, D., Ripepe, M., 2016. Conduit dynamics and post explosion degassing on Stromboli: A combined UV camera and numerical modeling treatment. Geophys. Res. Lett. 43, 5009–5016. https://doi.org/10.1002/2016GL069001

Pichavant, M., Pompilio, M., D´oriano, C., Dicarlo, I., 2011. Petrography, mineralogy and geochemistry of a primitive pumice from Stromboli: implications for the deep feeding system. Eur. J. Mineral. 23, 499–517. https://doi.org/10.1127/0935-1221/2011/0023-2109

Pioli, L., Pistolesi, M., Rosi, M., 2014. Transient explosions at open-vent volcanoes: The case of Stromboli (Italy). Geology 42, 863–866. https://doi.org/10.1130/G35844.1

738 Pistolesi, M., Donne, D.D., Pioli, L., Rosi, M., Ripepe, M., 2011. The 15 March 2007 explosive
739 crisis at Stromboli volcano, Italy: Assessing physical parameters through a multidisciplinary
740 approach. J. Geophys. Res. Solid Earth 116, 1–18. https://doi.org/10.1029/2011JB008527

741 Pistolesi, M., Rosi, M., Pioli, L., Renzulli, A., Bertagnini, A., Andronico, D., 2008. The paroxysmal
742 event and its deposits. Stromboli Volcano An Integr. Study 2002 - 2003 Eruption. Geophysica,
743 317–330. https://doi.org/10.1029/182GM26

744 Polacci, M., Baker, D.R., Mancini, L., Favretto, S., Hill, R.J., 2009. Vesiculation in magmas from
745 Stromboli and implications for normal Strombolian activity and paroxysmal explosions in
746 basaltic systems. J. Geophys. Res. Solid Earth 114, 1–14.
747 https://doi.org/10.1029/2008JB005672

748 Polacci, M., Corsaro, R.A., Andronico, D., 2006. Coupled textural and compositional
749 characterization of basaltic scoria: Insights into the transition from Strombolian to fire fountain
750 activity at Mount Etna, Italy. Geology 34, 201–204. https://doi.org/10.1130/G22318.1

751 Pompilio, M., Bertagnini, A., Métrich, N., 2012. Geochemical heterogeneities and dynamics of
752 magmas within the plumbing system of a persistently active volcano: Evidence from
753 Stromboli. Bull. Volcanol. 74, 881–894. https://doi.org/10.1007/s00445-011-0571-z

754 Ripepe, M., Harris, A.J.L., 2008. Dynamics of the 5 April 2003 explosive paroxysm observed at
755 Stromboli by a near-vent thermal, seismic and infrasonic array. Geophys. Res. Lett. 35, 4–9.
756 https://doi.org/10.1029/2007GL032533

757 Ripepe, M., Poggi, P., Braun, T., Gordeev, E., 1996. Infrasonic waves and volcanic tremor at
758 Stromboli 23, 181–184.

759 Rosi, M., Bertagnini, A., Harris, A.J.L., Pioli, L., Pistolesi, M., Ripepe, M., 2006. A case history of
760 paroxysmal explosion at Stromboli: Timing and dynamics of the April 5, 2003 event. Earth
761 Planet. Sci. Lett. 243, 594–606. https://doi.org/10.1016/j.epsl.2006.01.035

762 Rosi, M., Bertagnini, A., Landi, P., 2000. Onset of the persistent activity at Stromboli volcano

(Italy). Bull. Volcanol. 62, 294–300. https://doi.org/10.1007/s004450000098

Rosi, M., Pistolesi, M., Bertagnini, A., Landi, P., Pompilio, M., Di Roberto, A., 2013. Chapter 14 Stromboli volcano, Aeolian Islands (Italy): present eruptive activity and hazards. Geol. Soc. London, Mem. 37, 473–490. https://doi.org/10.1144/M37.14

Shea, T., Houghton, B.F., Gurioli, L., Cashman, K. V., Hammer, J.E., Hobden, B.J., 2010. Textural studies of vesicles in volcanic rocks: An integrated methodology. J. Volcanol. Geotherm. Res. 190, 271–289. https://doi.org/10.1016/j.jvolgeores.2009.12.003

Suckale, J., Keller, T., Cashman, K. V., Persson, P.O., 2016. Flow-to-fracture transition in a volcanic mush plug may govern normal eruptions at Stromboli. Geophys. Res. Lett. 43, 12,071-12,081. https://doi.org/10.1002/2016GL071501

Vergniolle, S., Brandeis, G., Mareschal, J., 1996. Strombolian explosions 2. Eruption dynamics determined from acoustic measurements. J. Geophys. Res. 101, 20449–20466. https://doi.org/10.1029/96JB01925Woitischek, J., Edmonds, M., Woods, A.W., 2020. The control of magma crystallinity on the fuctuations in gas composition at open vent basaltic volcanoes. Scientific Reports 10:14862 https://doi.org/10.1038/s41598-020-71667-7

Woitischek, J., Edmonds, M., Woods, A.W., 2020. The control of magma crystallinity on the fuctuations in gas composition at open vent basaltic volcanoes. Scientific Reports 10:14862 https://doi.org/10.1038/s41598-020-71667-7

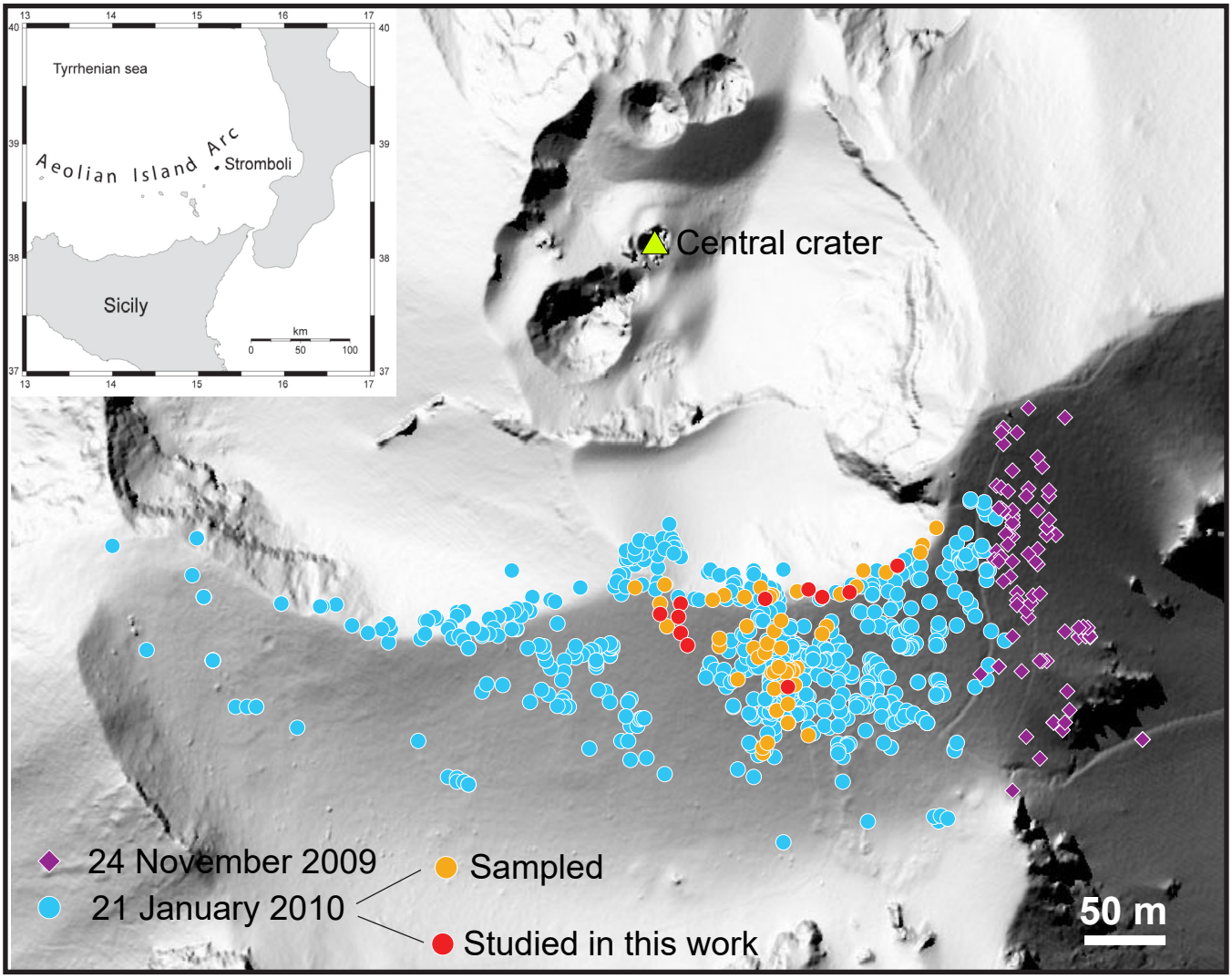
Tyrrhenian sea
Aeolian Island Arc
Stromboli
Sicily
km
0
50
100
13
14
15
16
17
40
39
38
37
Central crater
24 November 2009
21 January 2010
Sampled
Studied in this work
50 m

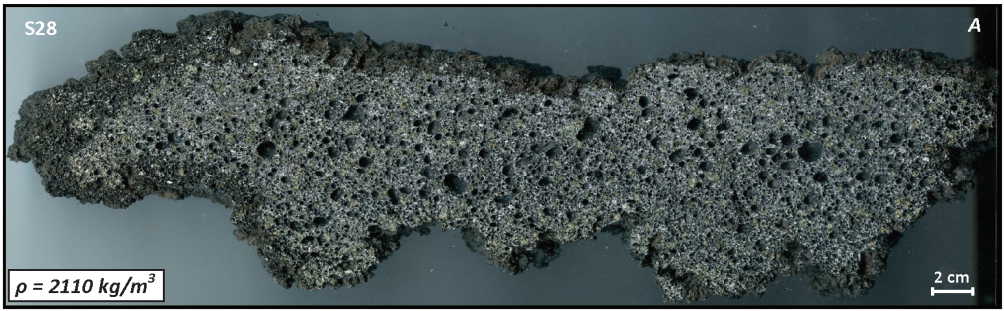
S28
A
ρ = 2110 kg/m3
2 cm

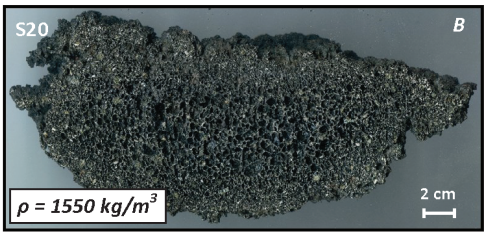
S20
B
ρ = 1550 kg/m3
2 cm

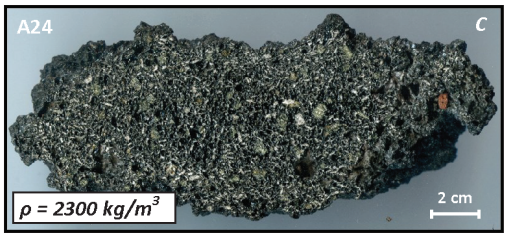
A24
C
ρ = 2300 kg/m3
2 cm

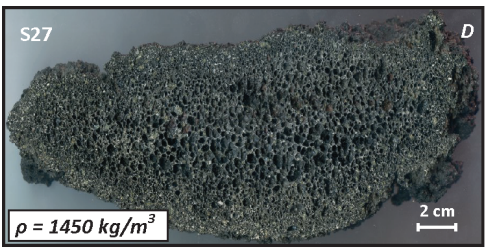
S27
D
ρ = 1450 kg/m3
2 cm


E
2 cm

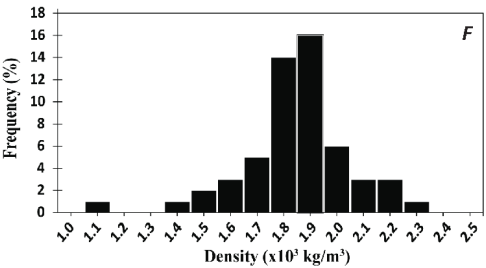
F
Frequency (%)
18
16
14
12
10
8
6
4
2
0
1.0
1.1
1.2
1.3
1.4
1.5
1.6
1.7
1.8
1.9
2.0
2.1
2.2
2.3
2.4
2.5
Density (x10³ kg/m³)

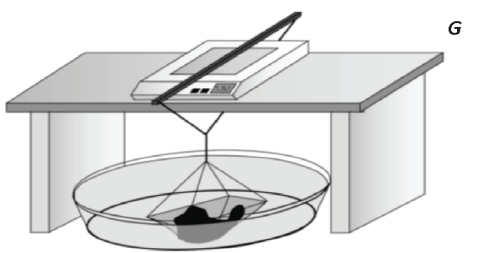
G

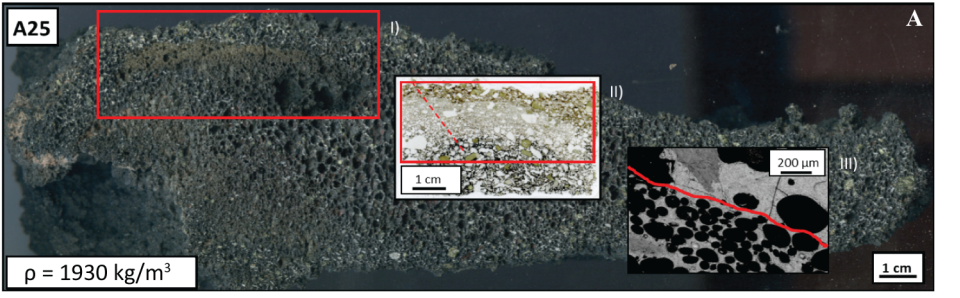
A25
A
I)
II)
III)
1 cm
200 µm
1 cm
ρ = 1930 kg/m³

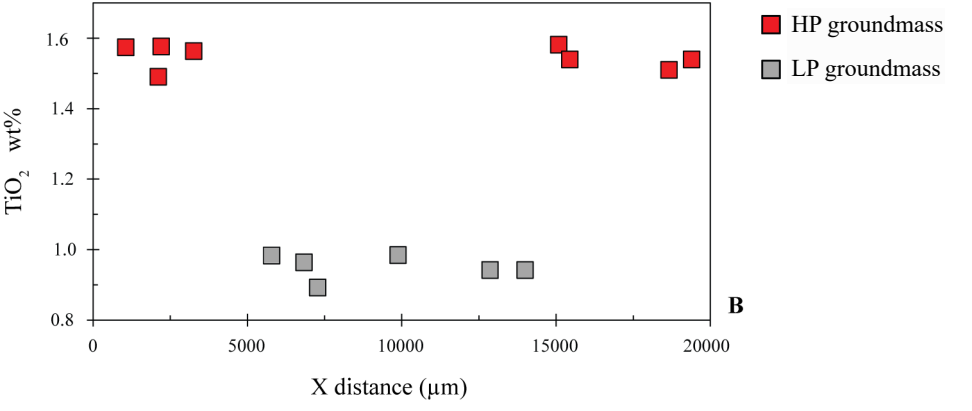
HP groundmass
LP groundmass
TiO2 wt%
1.6
1.4
1.2
1.0
0.8
0
5000
10000
15000
20000
X distance (µm)
B

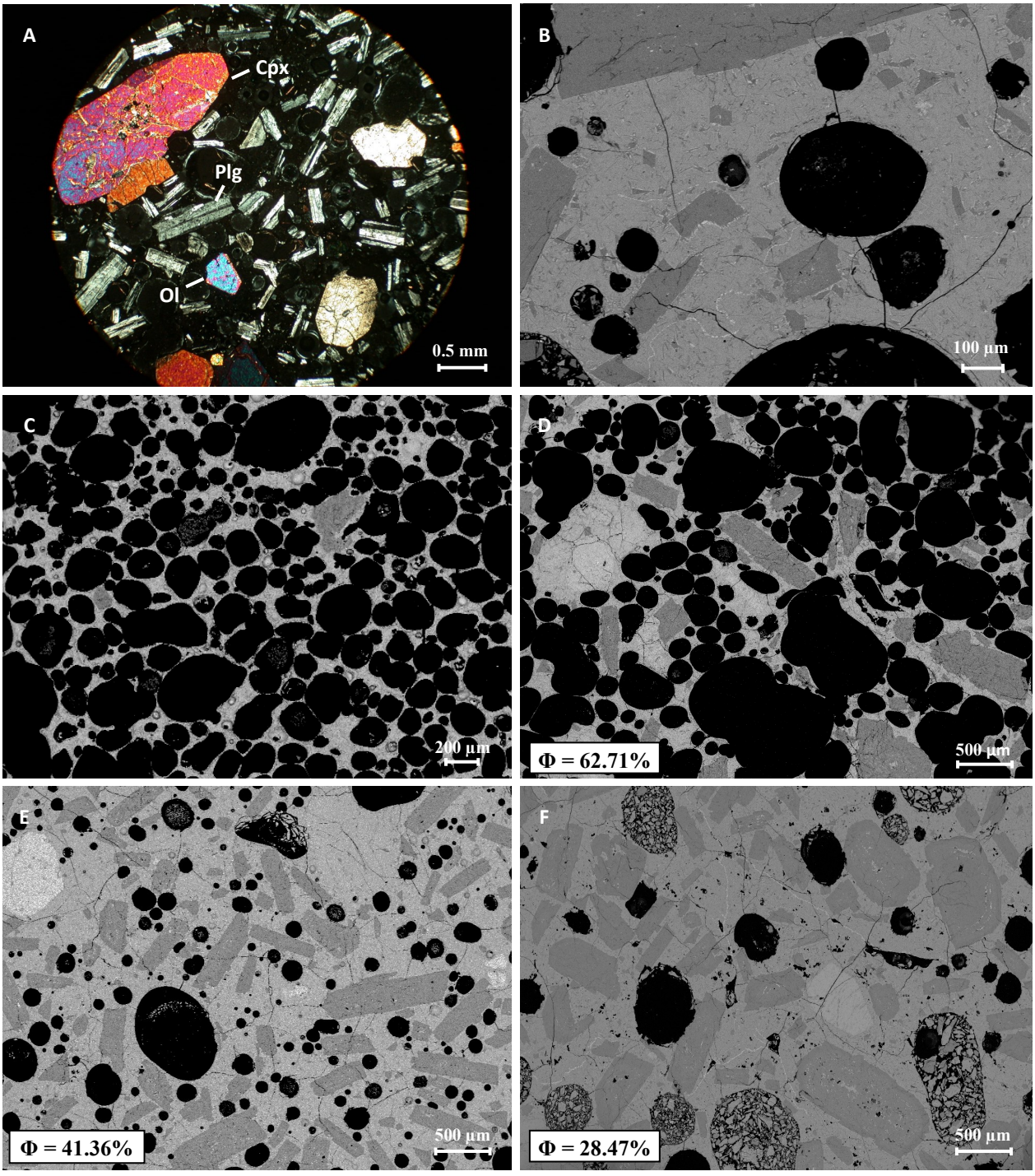
A
Cpx
Plg
Ol
0.5 mm
B
100 µm
C
200 µm
D
Φ = 62.71%
500 µm
E
Φ = 41.36%
500 µm
F
Φ = 28.47%
500 µm

Vesicle volume distributions (VVDs)

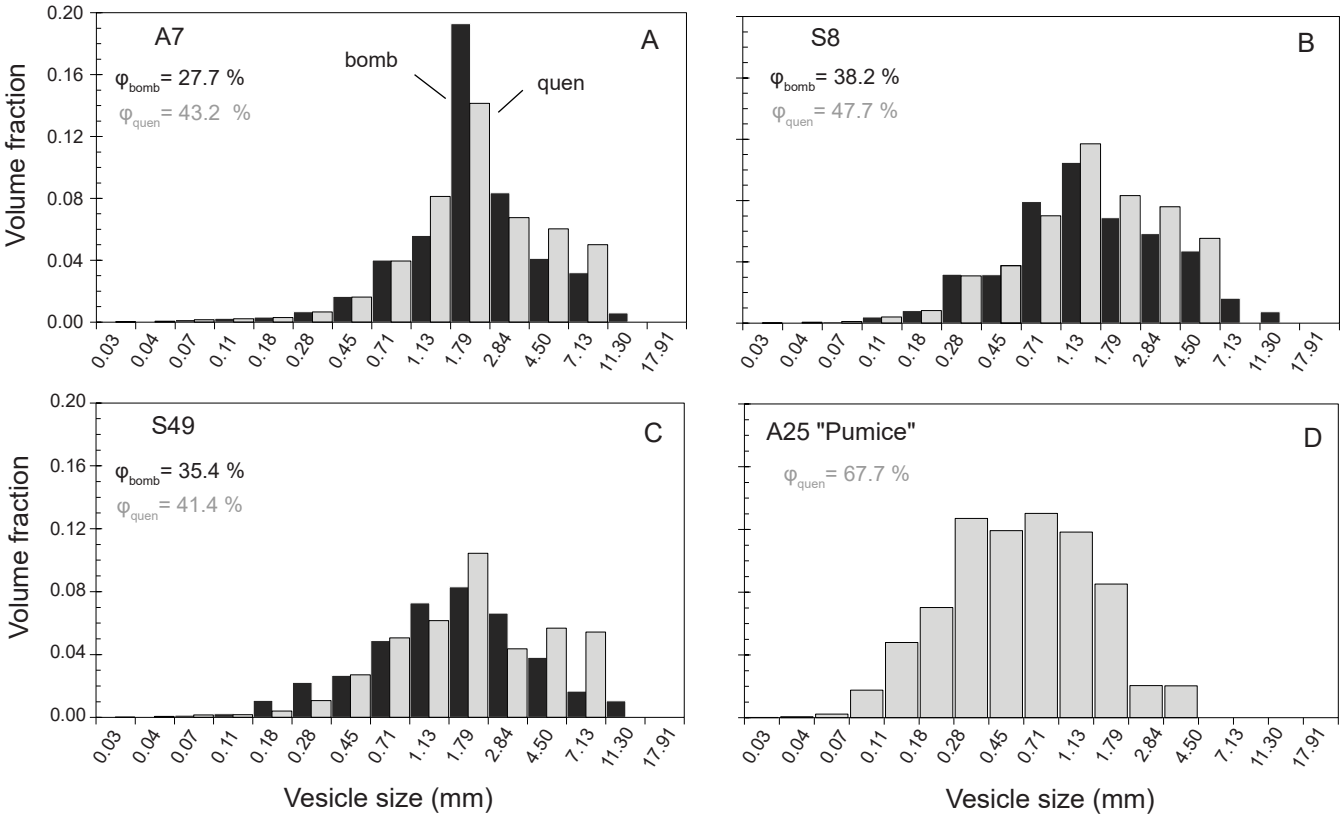

Crystal size distribution (CSDs)

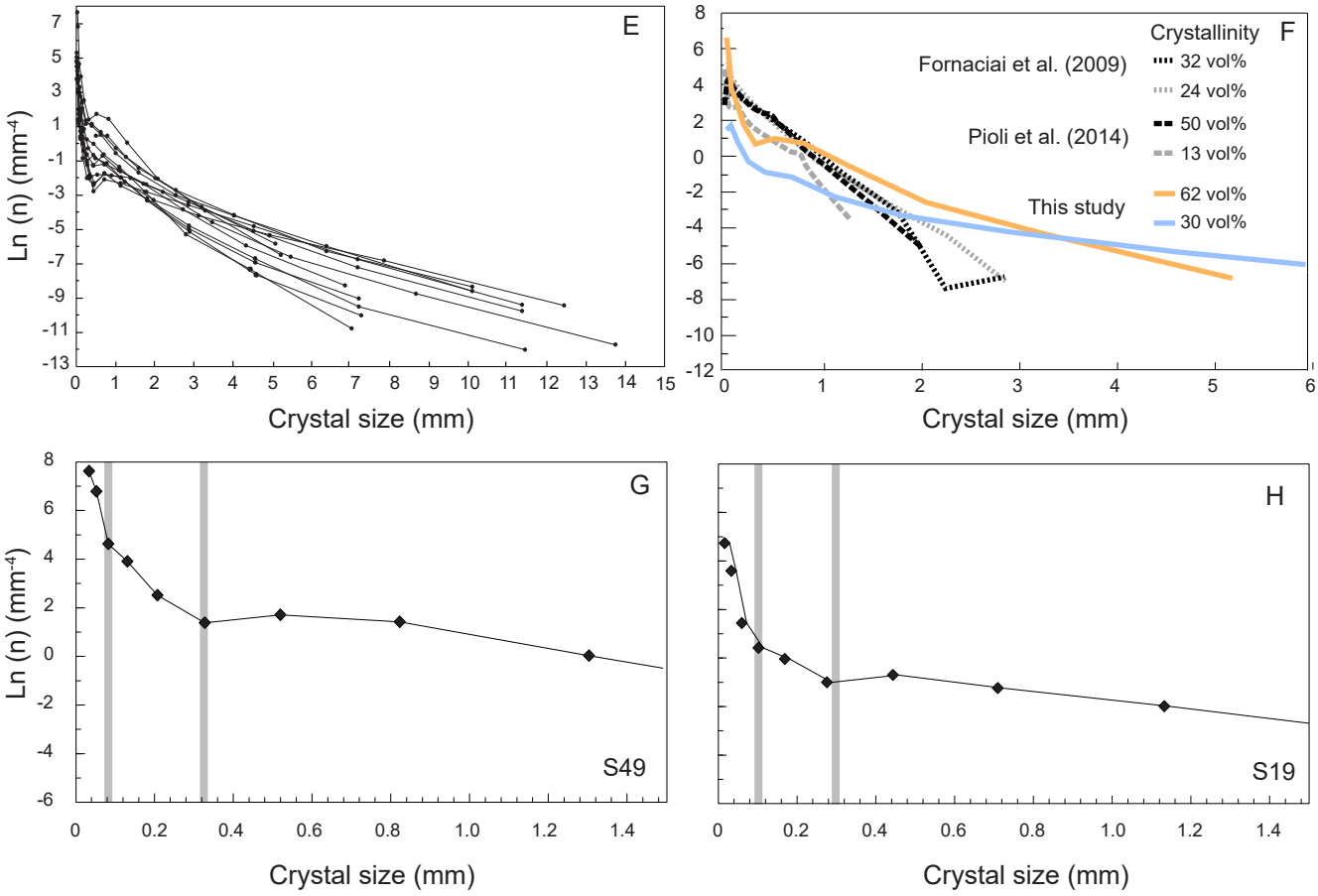

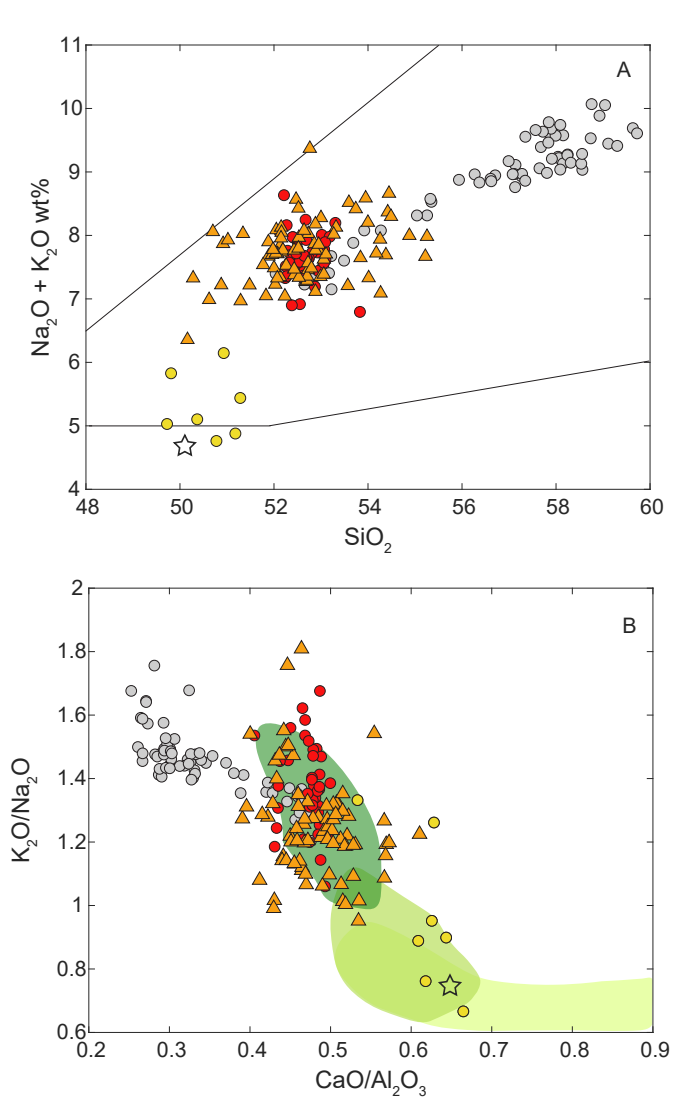
A
$Na_2O + K_2O$ wt%
SiO_2
B
K_2O/Na_2O
CaO/Al_2O_3
HP gm
LP gm
HP MIs
Gurioli et al. 2014
Bulk scoria
HP (MIs + gm) field*
LP gm field*
LP MIs field*

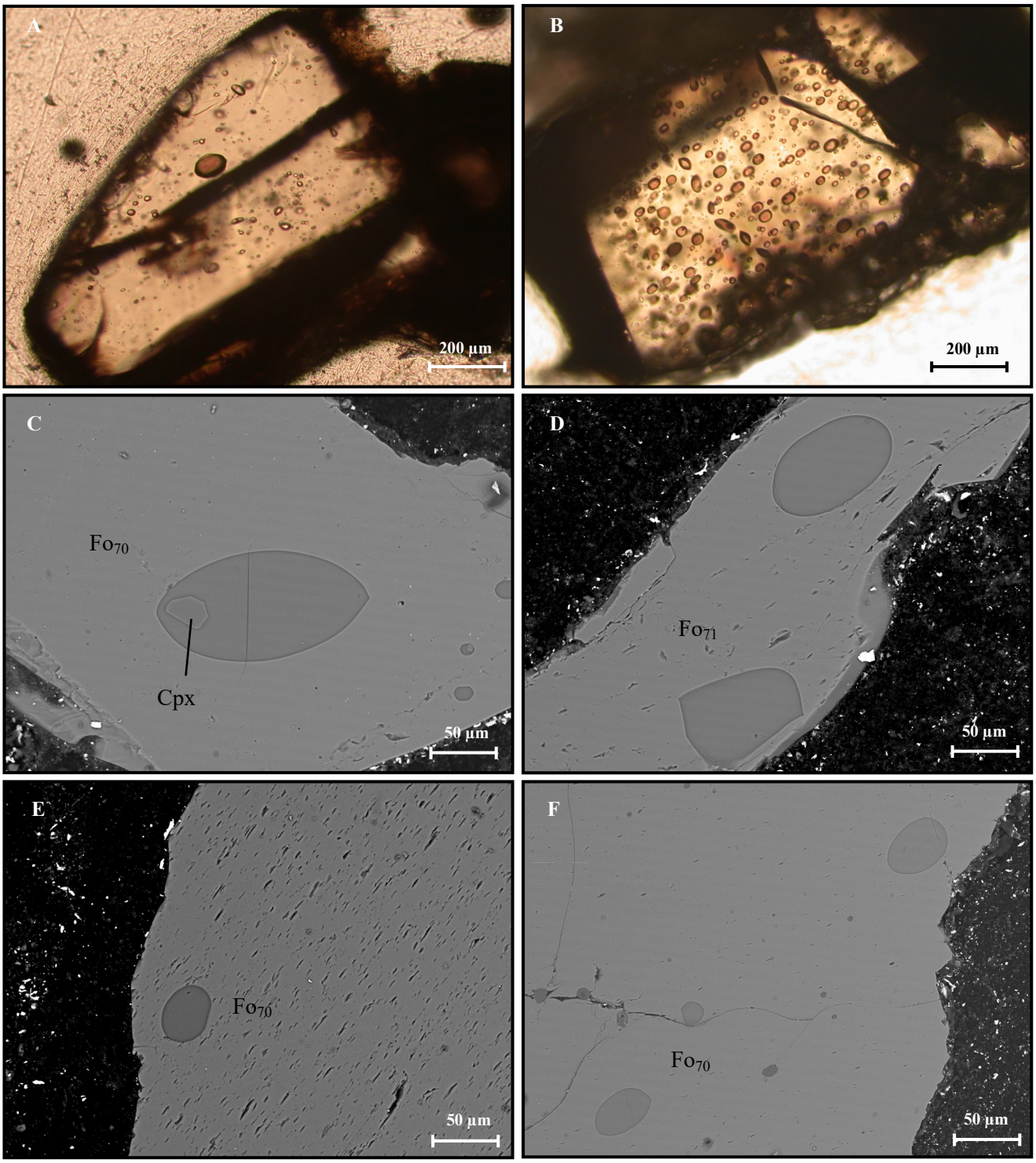
A
200 µm
B
200 µm
C
Fo70
Cpx
50 µm
D
Fo71
50 µm
E
Fo70
50 µm
F
Fo70
50 µm

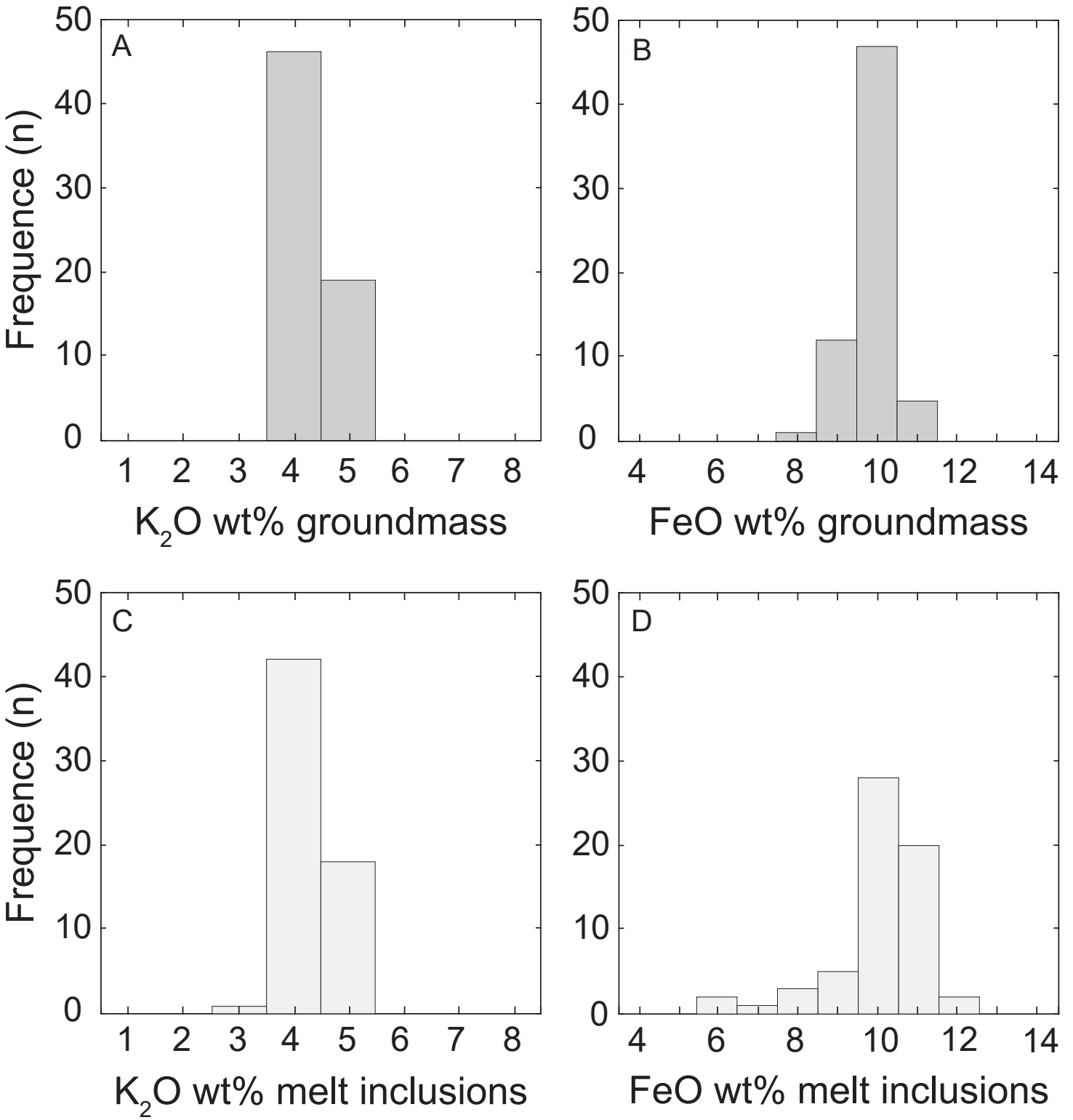
A
B
C
D
Frequence (n)
Frequence (n)
0
10
20
30
40
50
1
2
3
4
5
6
7
8
4
6
8
10
12
14
K2O wt% groundmass
FeO wt% groundmass
K2O wt% melt inclusions
FeO wt% melt inclusions

Table 1. Summary of the textural features of the 12 studied bombs. The table shows. for each sample: sample name (sample); measured whole density (ρ_w); measured density of quenched external slices (ρ_q); derived-whole density vesicularity (Φ_d); FOAMS-derived vesicularity (Φ_{FOAMS}) of the entire bomb; number of images processed for each sample (N_i); Number of vesicles analyzed for each sample (N_ves); number of crystals analyzed for each sample (N_ctx); crystallinity (Ctx); vesicle-free crystallinity, glass referred (Ctx_{corr}); vesicle free percentage of phenocrystals. microphenocrystals and microlites, respectively ($Pheno_{corr}$. $\mu pheno_{corr}$. $microlites_{corr}$); total volumetric number density of vesicles referenced to whole bomb (N_v); total volumetric number density of vesicles corrected for vesicularity and referred to melt only (N_v^{corr}).

Sample	ρ_w (kg/m^{-3})	ρ_q (kg/m^{-3})	Φ_d (vol %)	Φ_{FOAMS} (vol %)	N_i	N_ves	N_ctx	Ctx (%)	Ctx_{corr} (%)	$Pheno_{corr}$ (%)	$\mu pheno_{corr}$ (%)	$Microlites_{corr}$ (%)	N_V (mm^{-3})	N_v^{corr} (mm^{-3})
A23	1100	-	61.4	59.3	20	1331	259	23.6	61.3	39.5	15.3	6.5	90	225
S19	1370	1340	51.9	-	20	592	1210	30.0	62.5	36.5	9.9	16.1	1665	3350
S20	1550	1250	45.6	37.0	12	1949	903	28.4	52.2	31.6	4.7	15.9	328	581
S25	1670	1440	41.4	38.8	18	727	1177	28.1	48.0	27.3	6.7	14.0	719	1181
S38	1730	1680	39.3	28.7	18	854	1101	31.8	52.4	28.7	11.5	12.1	509	807
S8	1760	1490	38.2	44.1	11	1714	894	33.2	53.7	35.2	4.1	14.4	829	1298
S49	1840	1670	35.4	35.8	17	1576	701	27.8	43.0	24.6	7.5	11.0	725	1081
A20	1860	1460	34.7	41.3	20	776	607	35.0	53.6	28.2	14.4	11.0	1740	2578
A25 (scoria)	1930	-	32.3	51.3	11	334	592	20.5	30.3	20.4	6.6	3.3	555	792
A7	2060	1620	27.7	48.4	14	643	733	31.0	42.8	28.9	3.9	10.0	763	1017
S28-2	2110	1960	26.0	29.8	20	889	3248	36.9	49.8	32.7	3.6	13.5	1427	1861
A24	2300	1850	19.3	38.4	20	983	1273	37.6	46.6	28.9	4.9	12.9	608	727
A25 (pumice)	-	-	-	-	10	2024	63	0.5	1.7	0.5	1.0	0.1	1812	5612

	A24	*S29*			*S28*	*A7*	
	MI₁	*MI₁*	*MI₂*	*MI₃*	*MI₁*	*MI₁*	*MI₂*
SiO_2	52.62	52.46	50.73	51.66	52.34	51.74	51.49
TiO_2	1.53	1.81	1.77	1.57	1.84	1.79	1.64
Al_2O_3	15.67	15.71	15.23	15.85	15.57	16.16	15.50
FeO	8.34	7.98	9.02	8.52	8.44	8.32	8.68
Fe_2O_3	1.94	1.94	2.38	1.98	1.96	2.08	2.12
MnO	0.12	0.12	0.12	0.15	0.18	0.20	0.08
MgO	3.48	3.49	3.83	3.72	3.72	3.34	3.67
CaO	7.24	7.10	7.85	7.21	7.84	7.41	7.85
Na_2O	3.65	3.76	3.43	3.67	3.39	3.48	3.33
K2O	4.17	4.30	4.45	4.16	4.06	4.20	4.30
P_2O_5	0.52	0.69	0.67	0.79	0.08	0.68	0.72
S	0.07	0.09	0.09	0.11	0.08	0.12	0.06
Cl	0.23	0.20	0.10	0.16	0.23	0.13	0.20
H_2O	0.43	0.35	0.33	0.46	0.27	0.36	0.37
Sum	100	100	100	100	100	100	100
CaO/Al_2O_3	0.46	0.45	0.52	0.46	0.50	0.46	0.51
K_2O/Na_2O	1.14	1.14	1.30	1.13	1.20	1.21	1.29
Fo	70	70	70	72	70	71	71
PEP	0	0	0	1	0	1	2

Table 2. Major element and volatile content (wt%) of PEP-corrected olivine-hosted melt inclusions. % Fo: host olivine composition in mol %; PEP: post-entrapment processes (in %).